Journal of Biomechanics 48 (2015) 687–694

Contents lists available at ScienceDirect

Journal of Biomechanics

journal homepage: www.elsevier.com/locate/jbiomech
www.JBiomech.com

Wave intensity analysis in air-filled flexible vessels

Francesco Clavica [a], Kim H. Parker [b], Ashraf W. Khir [a,*]

[a] Brunel Institute for Bioengineering, Brunel University, Kingston Lane, Uxbridge, Middlesex UB8 3PH, UK
[b] Department of Bioengineering, Imperial College , London, UK

ARTICLE INFO

Article history:
Accepted 12 December 2014

Keywords:
Wave propagation
Wave speed
Air waves
flexible tubes
Wave intensity analysis

ABSTRACT

Wave intensity analysis (WIA) is an analytical technique generally used to investigate the propagation of waves in the cardiovascular system. Despite its increasing usage in the cardiovascular system, to our knowledge WIA has never been applied to the respiratory system. Given the analogies between arteries and airways (i.e. fluid flow in flexible vessels), the aim of this work is to test the applicability of WIA with gas flow instead of liquid flow. The models employed in this study are similar to earlier studies used for arterial investigations. Simultaneous pressure (P) and velocity (U) measurements were initially made in a single tube and then in several flexible tubes connected in series. Wave speed was calculated using the foot-to-foot method (c_f), which was used to separate analytically the measured P and U waveforms into their forward and backward components. Further, the data were used to calculate wave intensity, which was also separated into its forward and backward components. Although the measured wave speed was relatively high, the results showed that the onsets and the nature of reflections (compression/expansion) derived with WIA, corresponded well to those anticipated using the theory of waves in liquid-filled elastic tubes. On average the difference between the experimental and theoretical arrival time of reflection was 6.1% and 3.6% for the single vessel and multivessel experiment, respectively. The results suggest that WIA can provide relatively accurate information on reflections in air-filled flexible tubes, warranting further studies to explore the full potential of this technique in the respiratory system.

1. Introduction

The phenomenon of wave propagation in arteries has been extensively investigated experimentally (*in vivo* as well as *in vitro* studies) (Matthys et al., 2007; Feng and Khir, 2008; Parker and Jones, 1990) and computational models of pulse waves, propagating in the arterial network, have been developed with the arteries (or model arteries) considered as elastic tubes filled with blood (or water) (Sherwin et al., 2003; Alastruey et al., 2009; Alastruey et al., 2008; Formaggia et al., 2003). Wave intensity analysis (WIA) is a time domain analytical technique that was introduced by Parker and Jones (1990) for studying arterial waves. Although the mathematical derivation of WIA is quite complex involving the use of the method of characteristics to solve the 1-D conservation of mass and momentum equations, the results are very intuitive. Using WIA, it is possible to separate the forward and backward contribution of pressure (P) and velocity (U) waveforms for a straightforward interpretation of the existence and the distance of reflection sites (e.g. obstructions, bifurcations) by simply looking at the amplitude and arrival time of reflected waves, respectively.

The respiratory system, like the arterial system, is a branching network of elastic tubes where bifurcations, obstructions and the bronchioles represent the main source of reflections. Currently there are two main techniques for the diagnosis of airways obstruction and for a general assessment of respiratory mechanics; the forced oscillation technique (FOT) and the impulse oscillometry system (IOS), both measuring the response to artificial pulses induced at the mouth of the patient. The basic concept for these techniques relies on forcing an external signal that can be (i) sinusoidal (mono or multi frequency) for FOT (Oostveen et al., 2003) or (ii) an aperiodic single impulse of alternative direction for IOS (Smith et al., 2005). However, the results can be difficult to interpret since FOT and IOS provide information about the impedance of the overall respiratory system in the frequency domain; information about the location of single reflection sites is very difficult to determine unambiguously. It seems therefore reasonable to consider the use of WIA, which is a temporal rather than a frequency based analysis, as a possible tool to investigate the phenomenon of propagation and reflection of waves. We consider the waves involving the exchange of energy between the elastic airway walls and the kinetic energy of the air in lungs (i.e. air-wall waves), in which context the analysis of reflected air-wall waves could be applied, for example, as a non-invasive tool for the detection of bronchial obstruction. Therefore, the aim of this work is to test the applicability of WIA in simple configurations using air-filled flexible tubes. In this respect continuous measurements of P and U, which are the signals acquired routinely with IOS and FOT, are used to calculated wave intensity in simplified experimental models of airways. First a

* Corresponding author: Tel.: +44 1895265857; fax: +44 1895274608.
E-mail address: ashraf.khir@brunel.ac.uk (A.W. Khir).

http://dx.doi.org/10.1016/j.jbiomech.2014.12.037
0021-9290/

single distensible tube (single vessel experiment) is considered then the study is extended to three tubes connected in series (multivessel experiment).

2. Methodology

2.1. Wave intensity analysis: basic principles

WIA considers pressure and velocity waveforms as successive wavefronts, and wave intensity (dI) is defined as

$$dI = dPdU \tag{1}$$

Where dP and dU are respectively the change of pressure and velocity during a sample time, measured simultaneously at the same site. Assuming that forward and backward waves interact linearly, we can write

$$dP = dP_+ + dP_- \tag{2a}$$

$$dU = dU_+ + dU_- \tag{2b}$$

where the subscripts $(+)$ and $(-)$ denote the forward and backward directions respectively.

With a knowledge of wave speed (c), the fluid density (ρ), the Water hammer equation derived from the conservation of mass and momentum across the wavefornt in the $(+)$ and $(-)$ directions ($dP_\pm = \pm \rho c dU_\pm$) yields

$$dP_\pm = 1/2(dP \pm \rho c dU) \tag{3a}$$

$$dU_\pm = 1/2(dU \pm dP/\rho c). \tag{3b}$$

Integration of Eqs. (3a) and (3b) gives the pressure and velocity waveforms in the $(+)$ and $(-)$ direction.

$$P_+(t) = P_0 + \sum_{t=0}^{t} dP_+(t) \tag{4a}$$

$$P_-(t) = P_0 + \sum_{t=0}^{t} dP_-(t) \tag{4b}$$

$$U_+(t) = U_0 + \sum_{t=0}^{t} dU_+(t) \tag{4c}$$

$$U_-(t) = U_0 + \sum_{t=0}^{t} dU_-(t) \tag{4d}$$

where t is time, P_0, U_0 are the integration constants, chosen as pressure and velocity at $t=0$, when $P(0) = P_{+0}(0) + P_{-0}(0)$ and similarly $U(0) = U_{+0}(0) + U_{-0}(0)$

If we assume that the $(+)$ and $(-)$ waves interact linearly (additive), then the forward and backward wave intensities ($dI_\pm$) can be calculated (Parker and Jones, 1990)

$$dI_\pm = \pm \frac{1}{4\rho c}(dP \pm \rho c dU)^2. \tag{5}$$

Waves can be classified into four groups i.e. compression and expansion, according to their effect on pressure, and based on the direction of propagation. Compression waves induce an increase in pressure while expansion waves induce a decrease in pressure, in both the $(+)$ and $(-)$ directions (Feng and Khir, 2008). Forward compression waves (FCW) and backward expansion waves (BEW) induce an increase in velocity while forward expansion waves (FEW) and backward compression waves (BCW) induce a decrease in velocity (Table 1). The input pulse used in our experiments can be interpreted as a sequence of two forward waves (Feng and Khir, 2008): the first half of the waveform is a FCW since pressure increases, and the second half is FEW since pressure decrease.

Table 1
Wave classification: compression and expansion waves can propagate in forward or backward direction with different effects on pressure (dP) and velocity (dU) differences and consequently on dI (Feng and Khir, 2008). $dI > 0$ for forward travelling waves and $dI < 0$ for backward travelling waves.

Waves	dP	dU	dI	Flow direction
Compression	>0	>0	>0	FORWARD
Expansion	<0	<0	>0	
Compression	>0	<0	<0	BACKWARD
Expansion	<0	>0	<0	

3. Experimental set-up

A schematic of the experimental set-up is shown in Fig. 1. The simultaneous measurements of P and U in a single location (T connector in Fig. 1) as required by WIA were taken at 0.41 and 0.36 m away from the inlet for the single and multivessel experiment respectively (Fig. 2). We note the distance between the measurement point and the inlet is less than the theoretical entrance length (for both laminar and turbulent conditions) (Johnson, 1998) as would also be the case for measurements in the trachea. We decided not to use flow straighteners to avoid generating unwanted reflections.

The internal pressure of an air compressor (model 4-4, JUN-AIR, Denmark) was set at 4 atm. The compressor was attached to the inlet of a fast-switching solenoid valve (MHE3 FESTO, Germany), whose output was connected to the inlet of the tube system (Fig. 1B). Amplitude and duration of the initial pulse were controlled by regulating the pressure in the air compressor and the period of time that the solenoid valve was open, respectively. The opening duration of the solenoid valve and therefore the duration of the initial pulse was set at 15 ms for the single vessel experiment and 10 ms for the multivessel experiment. The peak of the initial pulse was 267 ± 7 Pa for the single vessel experiment and 705 ± 14 Pa for the multivessel experiment, similar in magnitude to those used in IOS (Smith et al., 2005; Ramos et al., 2010).

3.1. Flexible tubes

Four different flexible tubes were considered: a latex tube (LXT), a rubber tube (RT) and two silicon tubes denoted as ST1 and ST2. Table 2 shows the geometrical and mechanical properties of the tubes which, as far as we could determine, were uniform along their length. Young's modulus (E) was measured using tensile tests in the range 0–10% of strain. The rubber and the silicone tubes did not collapse at zero transmural pressure (under their own weight) whereas the latex tube did collapse. The wall thickness (h) of all tubes was measured using a digital caliper at zero transmural pressure (assuming h constant). The diameters (D) for rubber and silicon tubes were measured at zero transmural pressure while for the latex tube an internal pressure of 800 Pa was used, i.e. the pressure at which the latex tube first reached a circular cross-sectional area along its length.

3.2. Velocity and pressure measurements

The velocity probe used in the experiments was a split-fiber straight probe (55R55; Dantec Dynamics, Denmark). This probe was chosen as it allows for the measurement of the bidirectional flow, afforded by its two sensors. The probe was inserted in the tube using a rigid T connector on the axis of the lumen (Fig. 1D). The length of the connector (0.09 m) was assumed negligible compared to the length of the flexible tube. The measurement of the absolute value of velocity, in split fiber probes, is based on a modification of King's law (Helle, 1993)

$$E_1^2 + E_2^2 = A + B|U|^n \tag{6}$$

where E_1 and E_2 are the voltages of the two sensors. A, B and n are constant determined with the calibration process, which was conducted using a Streamline Pro Automatic Calibrator (Dantec Dynamics, Denmark). The plane of the probe splits was placed at the tube axis perpendicular to the direction of the mean flow (Bruun, 1995; Kiya and Sasaki, 1983), the flow direction was determined by comparing the voltages from the two sensors ($E_1 - E_2$), as suggested by Ra et al. (1990).

The pressure was measured using a 5 F transducer-tipped catheters (Gaeltec, Isle of Skye, UK) for the single vessel experiment and a 5 F transducer catheter (model SPC-760 Millar Instrument Inc, USA) for the multivessel experiment. The pressure catheter was inserted from the tube inlet (Fig. 1B) until its tip reached the T-connector to have P and U measured at the same location as required by WIA.

The signals were digitalized through a data acquisition board (DAQ) (National Instrument, USA), acquired using a custom written LabVIEW (National Instrument, USA) and smoothened with a third order Savitzky–Golay filter (frame size: 15 sample points) in Matlab (Mathworks Inc., USA). Data were sampled at either 2 kHz or 20 kHz.

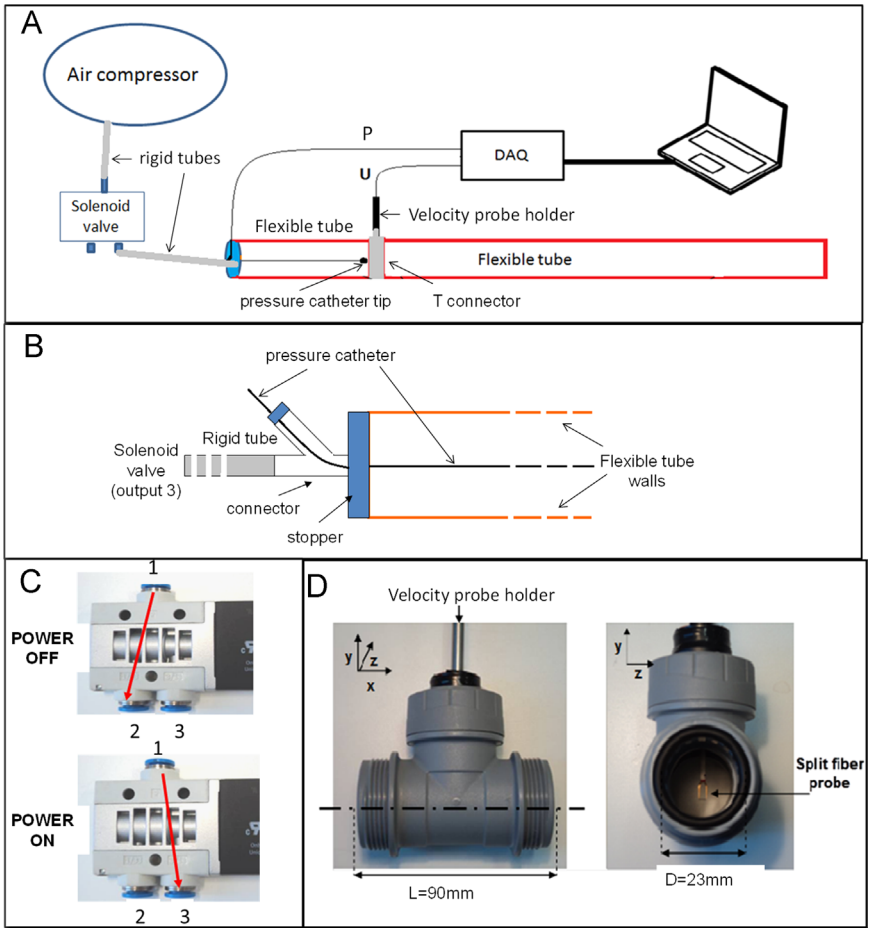

Fig. 1. (A) Schematic of the experimental set-up. Pressure (P) and velocity (U) signals were measured at the same location (T connector). DAQ=data acquisition board. (B) Schematic of the connections of the solenoid valve and pressure catheter to the inlet of the flexible tube. (C) Working principle of the solenoid valve in the two power configurations (off and on). Air pulse was generated by switching the power ON to connect the valve input 1 with output 3 (1 is the input connected to the air compressor, 2 is a blocked output and 3 is the output connected to the flexible tube). (D) T connector used to insert the split fiber probe into the lumen of the flexible tube.

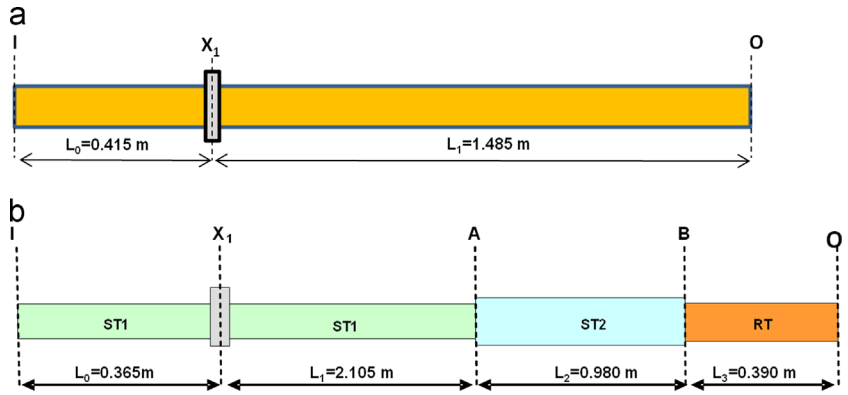

Fig. 2. (a) Schematic of the single vessel experiment and (b) schematic of the multivessel experiment. I and O are respectively the inlet and outlet of the tubes, A and B denote the tube junctions. L_i defines the length of the ith tube. Pressure and velocity measurements were at site X_1.

Table 2
Geometrical and mechanical properties of the flexible tubes used in the experiments ($N=4$): internal diameter (D), wall thickness (h), Young's modulus (E) and collapsibility/non-collapsibility behaviour of tubes at zero transmural pressure.

	D (mm)	h (mm)	E (MPa)	Collapsible tube?
LXT	32.1 ± 0.7	0.33 ± 0.02	0.68	YES
RT	21.0 ± 0.6	1.58 ± 0.20	1.35	NO
ST1	17.3 ± 0.1	2.59 ± 0.06	1.76	NO
ST2	29.7 ± 0.4	1.63 ± 0.11	1.81	NO

3.3. Single vessel experiment

A schematic of the set-up for the single vessel experiment is shown in Fig. 2a. The latex tube (LXT) was inflated with an initial constant pressure (P_0=800 Pa) before the experiment to avoid self-excited oscillations of the tube wall (Oruç and Çarpinlioğlu, 2007). Pressure and velocity were sampled at 2 kHz. The outlet of the tube was blocked using a stopper (i.e. closed-end condition). The wave speed associated to LXT was determined using the foot-to-foot method (c_f) generating an initial pulse and measuring the difference in time between the rise in pressure (the first sampling point where P becomes greater than the background noise) in two locations inside the latex tube. The first location was the T connector as in Fig. 1A

then at a distance of 1 m a second pressure catheter was inserted from the tube outlet (second location).

3.4. Multivessel experiment

The wave speed was determined in each tube with the foot-to-foot method in the same way as for LXT. The tubes were then assembled by gluing them together end to end. A schematic of the set-up for the multivessel experiment is shown in Fig. 2b, which also shows the sequence of the tubes: ST1–ST2–RT. Two configurations were considered for the multivessel experiment: open-end and closed-end conditions, which should be associated with a terminal reflection coefficient -1 and $+1$ (in 'O' position, Fig. 2b). Since the average wave speed for this experiment was much higher than in the single vessel experiment (because of the stiffer tubes), the sampling frequency was increased to 20 kHz.

3.5. Wave paths and arrival time

Considering a wave travelling along N tubes, it is possible to calculate the theoretical arrival time (t_t) of the reflected wave at the measurement site X_1 if the wave speed and length are known for each tube.

$$t_t = \sum_{i=1}^{N} \frac{2L_i}{c_i} \tag{7}$$

where L_i and c_i are respectively the length and wave speed of the ith tube. The theoretical arrival time of reflected wave (t_t) is calculated assuming $c_i = c_f$ in Eq. (7). The experimental arrival time (t_e) of reflected wave was determined by eye from the dI_- waveform as the sampling point where the signal first exceeds the noise level.

4. Results

4.1. Single vessel experiment

The speed of sound in free air at the experimental conditions (at a temperature of 20 °C) is 343 m/s (Guelke and Bunn, 1981) and the air density is 1.2 Kg/m^3. For the latex tube the mean value of the wave speed determined with the foot-to-foot method ($N=4$) was $c_f = 102 \pm 8$ m/s.

Measured P and U and their calculated forward and backward components, for the single vessel experiment, are shown in Fig. 3a and b. Net wave intensity (dI), forward (dI_+) and backward (dI_-) waveforms are also shown in Fig. 3c.

In Table 3 the theoretical arrival times t_t of reflected and re-reflected waves are compared with the experimental arrival times (t_e) determined using WIA.

Changes of pressure, velocity and wave intensity waveforms coincide with good accuracy to the predicted times t_t indicated by the arrows in Fig. 3. The BCW, produced by the reflection from the closed end, induced an increase in pressure (Fig. 3a) and a decrease in velocity (Fig. 3b) as indicated by the solid arrow. Once this wave is re-reflected from the inlet (in the forward direction), it generates an increase in pressure (P_+) and an increase in velocity (U_+), with its arrival at the measurement site, indicated by the dashed arrow. Notably the wave intensity in Fig. 3c provides a very clear indication of the behaviour of the waves. Recalling that $dI > 0$ for forward waves and $dI < 0$ for backward waves (Table 1), after the passage of the initial waves (FCW and FEW) $dI = 0$ until the arrival of the reflected BCW and BEW. Because the solenoid valve is closed, when the backward waves reach the inlet of the tube they are re-reflected as another FCW' and

Table 3
Single vessel experiment: arrival times of reflected and re-reflected waves. The theoretical arrival times (t_t) of reflected waves from the tube closed outlet (BCW and BEW) and re-reflected from the tube inlet (FCW' and FEW') are calculated considering $c_i = c_f = 102$ m/s in Eq. (7). t_t are compared with the experimental times (t_e) derived from the onset of the reflected waves in the wave intensity waveform (Fig. 3c). The percentage error (E_e%) between theoretical and experimental timing is also reported.

Wave	t_t (ms)	t_e (ms)	$E_e\% = \left\lvert \frac{t_e - t_t}{t_e} \right\rvert 100$
BCW	29.1	29.0	0.3
BEW	40.1	36.5	9.8
FCW'	37.2	38.0	2.1
FEW'	48.2	43.0	12.1

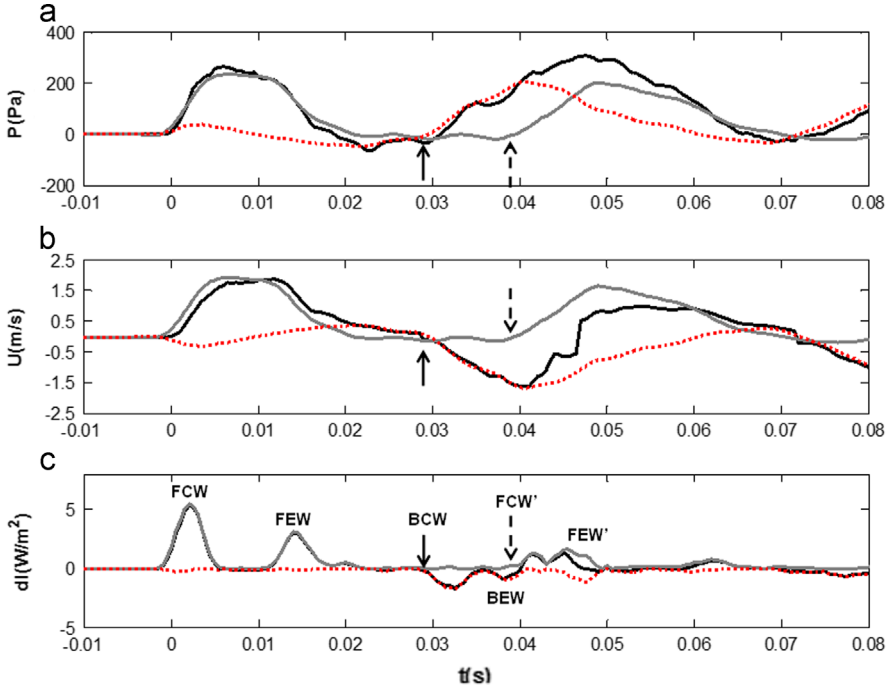

Fig. 3. Single vessel experiment: (a) pressure, (b) velocity and (c) wave intensity waveforms. The net waveforms of P, U and dI are shown in black, $c_f = 102$ m/s is used for the separations. Forward waveforms are shown in grey and the backward in dashed line. The solid arrow indicates the theoretical arrival time ($t_t = 29.1$ ms) of the BCW (i.e. FCW reflected backward from the tube outlet), the dashed arrow indicates the arrival ($t_t = 37.2$ ms) of the same wave re-reflected forward from the inlet (FCW'). C) The initial forward FCW and FEW are reflected from the closed outlet of the tube generating two backward travelling waves (BCW and BEW) which are then re-reflected forward from the closed inlet of the tube (FCW' and FEW').

FEW' (the apostrophe is used to distinguish them from the initial waves). Because the distance from the inlet to the measurement site is fairly short, we see that the re-reflected wave arrives before the reflected BEW has fully passed, resulting in an overlap of the negative peak of BEW and the positive peak of FCW'.

4.2. Multivessel experiment

For the multivessel experiment the mean values of wave speed for each tube determined using the foot-to-foot method were: 328 ± 3 m/s for ST1, 282 ± 19 m/s for ST2 and 277 ± 5 m/s for RT. A comparison between the closed-end and open-end configurations of P and U waveforms for the multivessel experiment is shown in Fig. 4. A clear separation of the two pressure waveforms appears at the calculated t_t of the O wave, with P increasing for the closed end condition and P reduced for the open end condition. The velocity waveforms of the two configurations also separate distinctly at approximately t_t of the O wave with the velocity increasing in the open end condition and decreasing in closed end condition. P, U and dI waveforms (associated to the closed-end configuration) and their decomposition into their forward and backward components are shown in Fig. 5. Note that in this experiment, due to the overlap of the waves reflected from the multiple reflection sites resulting from the high wave speeds, we limited our analysis only to the first reflections of the initial FCW from the A, B and O reflection sites (Fig. 2b).

The two reflection coefficients (R), in the forward direction, at the tube junctions (i.e. A and in B) were respectively -0.54 and $+0.32$ (i.e. $R=(A_0/C_0-A_1/C_1)/(A_0/C_0+A_1/C_1)$, where A and C are the area and the wave speed upstream 0, and downstream 1 of the discontinuity). Substantial changes in the waveforms of Fig. 5 occur approximately at the theoretical arrival times of the reflected waves, indicated by the arrows. Comparisons between the theoretical and experimental arrival time of the reflected waves are shown in Table 4.

5. Discussion

In this work, air was treated dynamically as an incompressible fluid since the calculated Mach number in both experiments was much lower than 0.3 (Nguyen, 2006) which is also the case in the human bronchial tree. The velocity of air is approximately 1 m/s during normal breathing and it can reach 50 m/s during sneezing (Xie et al., 2007). In our experiments the peak Mach number based on the peak velocity of ~1.8 m/s was $Ma=0.005$, (Fig. 3b and Fig. 5b).

5.1. Wave speed in flexile tubes filled with gas

The wave speeds (determined by the foot-to-foot method) in our experiments using air were almost two orders of magnitude higher than those found in liquid-filled elastic tubes. This complicates the experimental procedure as a very short pulse and a very high temporal resolution of the detection system are required. The wave speeds are also less than the speed of sound in free air at the experimental conditions, which would be the relevant wave speed if the walls were rigid. The highest value of wave speed measured in our experiments was 328 m/s (for ST1) that is very close to the sound speed in free space at our experimental conditions (343 m/s at $T=20$ °C). It is well known that wave speed in rigid tubes approximately equals the sound speed (Korteweg, 1878; Guelke and Bunn, 1981) independently from the area and the shape of the tube cross-section (Rice, 1980). We therefore believe that having rigid tubes in our system, to simulate stiffer vessels of the bronchial tree, will only shift the value of wave speed for the rigid tubes to 343 m/s, and is not expected to affect the interpretation of the results.

Jackson et al. (1977) were able to derive the change of characteristic impedances by analysing the acoustic reflections measured at the mouth. Cross-sectional areas versus distance were derived for upper airways, using the algorithm of Ware and Aki (1969). The main limitations of their work were associated with the assumption of wall rigidity (Fredberg et al., 1980; Louis et al., 1994) for all the upper airways. This assumption was considered responsible for the large overestimation of the cross-sectional area of the airways (Sidell and Fredberg, 1978). According to our findings, their assumption also affects strongly the determination of the distance of the reflection site: using the speed of sound instead of c_f results in a large overestimation of the wave speed (up to 236% for the latex tube which is the most flexible tube in our experiment).

We also calculated the wave speed using the PU-loop method, according to Khir et al. (2001) (results not shown). The resulting

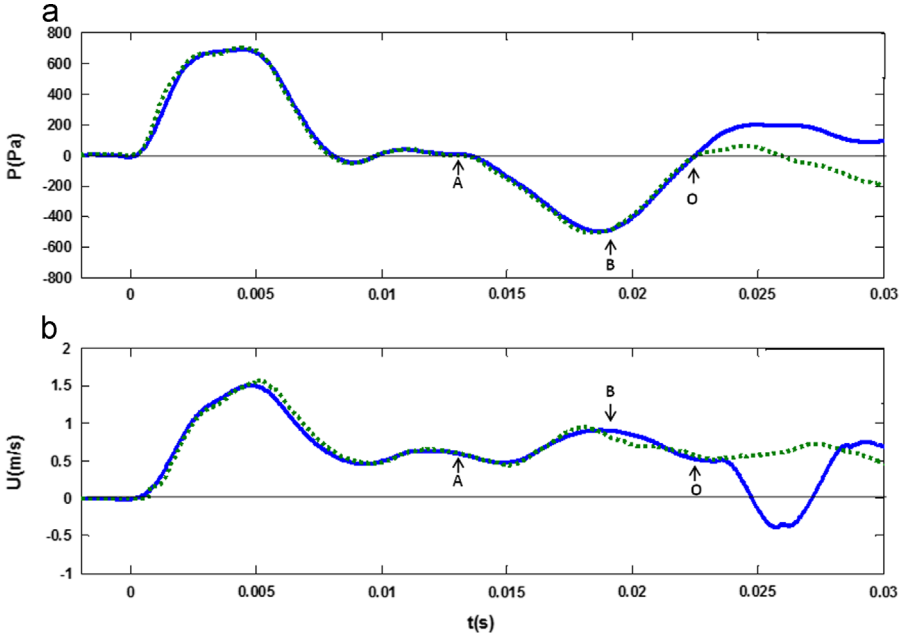

Fig. 4. Multivessel experiment: measured P and U at position X_1 according to closed-end (continuous line) and open-end (dashed line). The arrows indicate the theoretical arrival times (t_t) of the BCW waves (initial FCW reflected from the two junctions A, and B and the outlet O which was either closed or open, Fig. 2b) according to the timing given in Table 4.

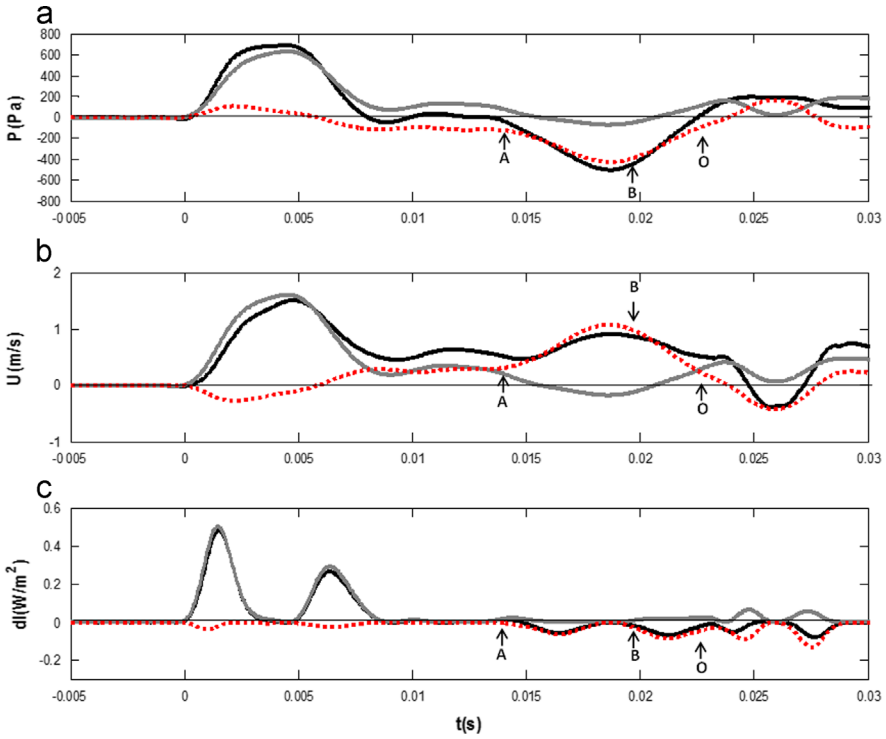

Fig. 5. Multivessel experiment for the closed outlet case: separation of measured *P*, *U* and calculated *dI* into their forward and backward components. *P*, *U* and *dI* are shown in black. c_f=328 m/s is used for the separations. The forward waveforms (+) are shown in grey and the backward (−) in dashed line. The arrows indicate the theoretical arrival time (t_t) of the first BCW (i.e. reflected waves from the reflective sites: A, B and O of Fig. 2b according to the times given in Table 4).

Table 4
Multivessel experiment: arrival times of reflected waves. The theoretical arrival times (t_t) of reflected waves from the reflection sites A, B and O (Fig. 2b) are calculated from the c_f values determined for each tube using Eq. (7). t_t are compared with the experimental times (t_e) derived from the onset of the reflected waves in the wave intensity waveform (Fig. 5c). The percentage error (E_e%) between theoretical and experimental timing is also reported.

Wave	t_t (ms)	t_e (ms)	$E_e\% = \left\|\frac{t_e - t_t}{t_e}\right\| 100$
A	12.83	13.40	4.2
B	19.78	18.70	5.7
O	22.60	22.85	1.1

wave speed (N=5) was 105 ± 13 m/s and 308 ± 54 m/s for the single vessel (i.e. LTX) and the multivessel experiments (i.e. ST1), respectively. The results of the foot-to-foot method in the corresponding experiments are $c_f = 102 \pm 8$ m/s and $c_f = 328 \pm 3$ m/s, which shows a bigger discrepancy in the case of the multivessel experiment that we think could be due to (i) the higher rigidity of the tube, which makes the exact determination of wave speed more difficult, (ii) higher number of reflections which may have an effect on wave speed determination as recently demonstrated in water-filled flexible tubes (Borlotti et al., 2013).

5.2. Wave intensity analysis in gas

As far as we are aware, this is the first time WIA has been applied to air-filled elastic tubes. The main advantage of wave intensity analysis is that once the wave speed is known *P*, *U* and *dI* can be separated into their forward and backward components. The possibility of separating waves makes WIA very promising for application to the respiratory system as the contribution of the reflected waves generated by bronchial obstructions could be separated from the incident wave. The diameters, Young's modulus and wall thickness of our tubes (particularly RT and ST1) are comparable to the physiological data available in literature on human upper airways' morphology i.e. Weibel (1963) for diameters, Montaudon et al. (2007) for wall thickness, Young's modulus (E) defined according to the content of cartilage and soft tissue of each airway generation (Habib et al., 1994; Lambert et al., 1991; Wiggs et al., 1990). These data were also considered in our earlier computational works; Clavica et al. (2009, 2010).

The flow amplitude of the IOS impulse, commonly used in clinics, is approximately 0.3 l/s (Smith et al., 2005) and it generates a pressure pulse of around 120–200 Pa (Smith et al., 2005, Ramos et al., 2010). The amplitude of our impulses were similar in magnitude (i.e. the flow amplitudes were 1.2 l/s for single vessel and 0.35 l/s for multivessel experiments) while the corresponding pressure pulses were 267 Pa and 705 Pa for single and multivessel experiment. In our experiments the two initial forward waves are represented by the first two positive peaks in *dI* waveforms (Fig. 3c and Fig. 5c). Notably in the single vessel experiments it is possible to track the reflection and re-reflection of these two waves, first in the backward direction (dI_-) and then again in the forward direction (Fig. 3c). More complex reflections appear in the multivessel experiments because of the higher number of reflection sites and the larger wave speeds. Given, for example, the delay of ~5 ms between the FCW and the FEW we would expect the first BEW (from reflections site A) to reach the measurement site together with the BCW from site B. For this reason we expect that t_e shown in Table 4 may be affected by the combination of these two waves. The difference between t_e and t_t on average is 6.1% for the single vessel and 3.6% for the multivessel experiment. In the single vessel experiment the time differences appear lower for the reflected waves (with a maximum value of 9.8%) compared to 12.1% of the re-reflected waves. This may be explained by an increased effect of nonlinearities in re-reflected waves due to the longer distances that the re-reflected waves have travelled and the bigger number of reflections they have undergone.

The differences between *P* and *U* waveforms of the multivessel experiment in the open- and closed-end configurations (Fig. 4)

are particularly significant to study difference of the terminal reflection coefficient. The pulse introduced at the inlet was always a FCW followed by a FEW, but the nature of the backward reflected waves depended on the type of reflections. Considering for simplicity only the reflections from the outlet of the initial FCW (not the FEW): in open-end configuration the reflected wave was a backward expansion wave while in the closed end a backward compression wave. We have demonstrated that the principles of wave reflections and propagation in air are in line with the theoretical expectations (Table 1) as in our earlier studies where water was used (Feng and Khir, 2008; Khir and Parker, 2002).

In the present work we focused mainly on the arrival time of reflected waves, an analysis of wave dissipation in the gas case, as done by Feng et al. (2007) for the liquid case, will require future study. For example the ratio between the peak in pressure of the BCW and the peak in pressure of the initial FCW in Fig. 3a is 0.8 which is lower than the theoretical terminal reflection = 1.

5.3. Limitations

The experimental set-up used in this work may introduce some uncertainties, which could explain the discrepancies between the theoretical values of return times and experimental times. The effects due to the discontinuity introduced by the rigid T-connector are neglected in this work. The change of wall properties and cross-sectional area may affect the P and U measurements inside the T connectors and contribute to local flow disturbances.

Air flow in the human bronchial tree is undoubtedly much more complex than that in a series of tubes as considered in this work. However, our aim was to establish whether WIA can be used to determine the arrival time of reflected waves in response to an initial pulse similar to existing techniques for the diagnosis of respiratory diseases. We used much longer lengths of tubes than the physiological values, this was because we wanted to avoid excessive interference of waves for an easier interpretation of data.

6. Conclusion

An experimental set-up for the measurements of pressure and velocity in gas-filled flexible tubes has been developed. For flows in flexible tubes with Mach number < 0.3 the fluid can be treated as incompressible and WIA can determine the arrival time of reflected air waves and therefore the distance of a reflection site. The separation of forward and backward contribution in P and U waveforms indicates the positive/negative nature of the reflection site. Despite the simple configuration used in this work, compared to the complexity of human airways, the results are promising and warrant further investigations to establish the potential usefulness of WIA in the clinical setting.

Conflict of interest statement

The authors have no conflict of interest.

Acknowledgement

The authors would like to acknowledge Professor Colin Clark for offering some of the measurement equipment and for the useful technical discussions.

References

Alastruey, J., Parker, K.H., Peiro, J., Sherwin, S.J., 2008. Lumped parameter outflow models for 1-D blood flow simulations: effect on pulse waves and parameter estimation. Commun. Comput. Phys. 4, 317–336.
Alastruey, J., Parker, K.H., Peiró, J., Sherwin, S.J., 2009. Analysing the pattern of pulse waves in arterial networks: a time-domain study. J. Eng. Math. 64, 331–351.
Borlotti, A., Li, Y., Parker, K.H., Khir, A.W., 2013. Experimental evaluation of local wave speed in the presence of reflected waves. J. Biomech. 47, 87–95.
Bruun, H.H., 1995. Hot-wire Anemometry: Principles and Signal Analysis. 95. Oxford University Press, Oxford p. 75.
Clavica, F., Alastruey, J., Borlotti, A., Sherwin, S.J., Khir, A.W., 2010. One-dimensional computational model of pulse wave propagation in the human bronchial tree. In: Proceedings of the Annual International Conference of the IEEE Engineering in Medicine and Biology Society, EMBC, pp. 2473–2476.
Clavica, F., Alastruey, J., Sherwin, S.J., Khir, A.W., 2009. One-dimensional modelling of pulse wave propagation in human airway bifurcations in space-time variables. In: Proceedings of the Annual International Conference of the IEEE Engineering in Medicine and Biology Society, EMBC, 5482–5485.
Feng, J., Khir, A.W., 2008. The compression and expansion waves of the forward and backward flows: an in-vitro arterial model. Proc. Inst. Mech. Eng. Part H: J. Eng. Med. 222, 531–542.
Feng, J., Long, Q., Khir, A.W., 2007. Wave dissipation in flexible tube in the time domain, in vitro model of arterial waves. J. Biomech. 40, 2031–2038.
Formaggia, L., Lamponi, D., Quarteroni, A., 2003. One-dimensional models for blood flow in arteries. J. Eng. Math. 47, 251–276.
Fredberg, J.J., Wohl, M.E.B., Glass, G.M., Dorkin, H.L., 1980. Airway area by acoustic reflections measured at the mouth. J. Appl. Physiol. 48, 749–758.
Guelke, R.W., Bunn, A.E., 1981. Transmission-line theory applied to sound-wave propagation in tubes with compliant walls. Acustica 48, 101–106.
Habib, R.H., Chalker, R.B., Suki, B., Jackson, A.C., 1994. Airway geometry and wall mechanical properties estimated from subglottal input impedance in humans. J. Appl. Physiol. 77 (1), 441–451.
Helle, L., 1993. The use of a split-fibre probe for aerodynamic research. Dantec Information No. 12 February.
Jackson, A.C., Butler, J.P., Millet, E.J., 1977. Airway geometry by analysis of acoustic pulse response measurements. J. Appl. Physiol. Respir. Environ. Exerc. Physiol. 43, 523–536.
Johnson, R., 1998. The Handbook of Fluid Dynamics. CRC Press, p. 563.
Khir, A.W., O'brien, A., Gibbs, J.S.R., Parker, K.H., 2001. Determination of wave speed and wave separation in the arteries. J. Biomech. 34 (9), 1145–1155.
Khir, A.W., Parker, K.H., 2002. Measurements of wave speed and reflected waves in elastic tubes and bifurcations. J. Biomech. 35, 775–783.
Korteweg, D.J. 1878. Uber die Fortflanzungsgeschwindigkeit des schalles inelastischem rohern. Ann. Phys. Chem. (NS) 5, 525-542.
Kiya, M., Sasaki, K., 1983. Structure of a turbulent separation bubble. J. Fluid. Mech. 137, 83–113.
Lambert, R.K., Baile, E.M., Moreno, R., Bert, J., Pare, P.D., 1991. A method for estimating the Young's modulus of complete tracheal cartilage rings. J. Appl. Physiol. 70 (3), 1152–1159.
Louis, B., Glass, G.M., Fredberg, J.J., 1994. Pulmonary airway area by the two microphone acoustic reflection method. J. Appl. Physiol. 76, 2234–2240.
Matthys, K.S., Alastruey, J., Peiró, J., Khir, A.W., Segers, P., Verdonck, P.R., 2007. Pulse wave propagation in a model human arterial network: assessment of 1-D numerical simulations against in vitro measurements. J. Biomech. 40, 3476–3486.
Montaudon, M., Desbarats, P., Berger, P., de Dietrich, G., Marthan, R., Laurent, F., 2007. Assessment of bronchial wall thickness and lumen diameter in human adults using multi-detector computed tomography: comparison with theoretical models. J. Anat. 211, 579–588.
Nguyen, N., 2006. Fundamentals and Applications of Microfluidics. Artech House, Boston, Mass, London p. 497.
Oostveen, E., MacLeod, D., Lorino, H., Farre, R., Hantos, Z., Desager, K., 2003. The forced oscillation technique in clinical practice: methodology, recommendations and future developments. Eur. Respir. J. 22, 1026–1041.
Oruç, V., Çarpinlioğlu, M.Ö., 2007. A test rig for the investigation of airflow through collapsible tubes. Proc. Inst. Mech. Eng. Part C: J. Mech. Eng. Sci. 221, 275–280.
Parker, K.H., Jones, C.J.H., 1990. Forward and backward running waves in the arteries: analysis using the method of characteristics. J. Biomech. Eng. 112, 322–326.
Ra, S.H., Chang, P.K., Park, S.O., 1990. Measurement of the forward-flow fraction using a split film sensor. Exp. Fluids 10, 57–59.
Ramos, C., Nazeran, H., Goldman, M.D., Diong, B., 2010. Circuit analysis justifies a reduced Mead's model of the human respiratory impedance for impulse oscillometry data. In: Proceedings of the Annual International Conference of the IEEE Engineering in Medicine and Biology Society, EMBC, pp. 548–552.
Rice, D.A., 1980. Sound speed in the upper airways. J. Applied Physiol. Respir. Environ. Exer. Physiol. 49, 326–336.
Sherwin, S.J., Franke, V., Peiró, J., Parker, K., 2003. One-dimensional modelling of a vascular network in space-time variables. J. Eng. Math. 47, 217–250.
Sidell, R.S., Fredberg, J.J., 1978. Noninvasive inference of airway network geometry from broad-band lung reflection data. J. Biomech. Eng.—Trans. ASME 100, 131–138.

Smith, H.J., Reinhold, P., Goldman, M.D., 2005. Lung function testing. In: Forced oscillation technique and impulse oscillometry. European Respiratory Society Journals Ltd. pp. 72–105.
Xie, X., Li, Y., Chwang, A.T., Ho, P.L., Seto, W.H., 2007. How far droplets can move in indoor environments—revisiting the Wells evaporation-falling curve. Indoor Air 17, 211–225.
Ware, J., Aki, K., 1969. Continuous and discrete inverse-scattering problems in a stratified elastic medium. Acoust. Soc. Am.-J. 45, 911–921.
Weibel, E.R., 1963. Morphometry of the Human Lung. Springer-Verlag, Berlin.
Wiggs, B.R., Moreno, R., Hogg, J.C., Hillian., C., Pare, P.D., 1990. A model of the mechanics of airway narrowing. J. Appl. Physiol. 69 (3), 849–860.